Pendent Relay Enhances H_2O_2 Selectivity During Dioxygen Reduction Mediated by bpy-based Co-N_2O_2 Complexes

Asa W. Nichols[a], Emma N. Cook[a], Yunqiao J. Gan[b], Peter R. Miedaner[a], Julia M. Dressel[a], Diane A. Dickie[a], Hannah S. Shafaat[b], Charles W. Machan[a]*

[a]Department of Chemistry, University of Virginia, McCormick Rd, PO Box 400319, Charlottesville, Virginia 22904-4319, USA

[b]Department of Chemistry and Biochemistry, The Ohio State University, 100 W. 18th Ave., Columbus, OH 43210 USA

Keywords dioxygen, cobalt, homogeneous, catalysis, redox, mechanism

Abstract: Generally, cobalt-N_2O_2 complexes show selectivity for hydrogen peroxide during electrochemical dioxygen (O_2) reduction. We recently reported a Co(III)-N_2O_2 complex with a 2,2′-bipyridine-based ligand backbone which showed alternative selectivity: H_2O was observed as the primary reduction product from O_2 (71±5%) using decamethylferrocene as a chemical reductant and acetic acid as a proton donor in methanol solution. We hypothesized that the key selectivity difference in this case arises in part from increased favorability of protonation at the distal O position of the key intermediate Co(III)-hydroperoxide species. To interrogate this hypothesis, we have prepared a new Co(III) compound with which contains pendent –OMe groups poised to direct protonation towards the proximal O atom of this hydroperoxo intermediate. Mechanistic studies in acetonitrile solution reveal two regimes are possible in the catalytic response, dependent on added acid strength and the presence of the pendent proton donor relay. In the presence of stronger acids, the activity of the complex containing pendent relays becomes O_2 dependent, implying a shift to Co(III)-superoxide protonation as the rate-determining step. Interestingly, the inclusion of the relay results in primarily H_2O_2 production in MeCN, despite minimal difference between the standard reduction potentials of the three complexes tested. EPR spectroscopic studies indicate the formation of Co(III)-superoxide species in the presence of exogenous base, with greater O_2 reactivity observed in the presence of the pendent –OMe groups.

Introduction

The reduction of dioxygen (ORR) to water (H_2O, $4e^-$, $4H^+$) or hydrogen peroxide (H_2O_2, $2e^-$, $2H^+$) is important for the development of new technologies for energy storage, understanding dioxygen-dependent biological systems, and the development of new oxidative chemical transformations via reactive oxygen species.[1,2] Understanding reaction mechanisms and controlling selectivity between the two pathways is vital: for both energy storage and the biological systems like cytochrome *c* oxidase (C*c*O), H_2O is the ideal product.[3-5] In energy storage technologies, the generation of H_2O_2 or other reactive oxygen species can be damaging to the cell-dividing membranes.[3,4] While H_2O is the desired product for the study of energy conversion and biomimetic use of ORR to simultaneously drive chemical oxidation reactions, the selective generation of reactive oxygen species or hydrogen peroxide is an attractive route to the discovery of new direct oxidation reactions using O_2 as the terminal oxidant.[2]

The study of molecular Co complexes for the reduction of dioxygen (O_2) has been examined extensively with N_4 macrocyclic ligand frameworks, including derivatives of porphyrins,[6-16] corroles,[17,18] phthalocyanines[19-23], chlorins,[24,25] and cyclam,[13,26-30] with the majority demonstrating selectivity for H_2O_2. For certain catalysts, Brønsted acid-scaling relationships have been used to alter product

selectivity through thermodynamic bracketing; by thermodynamically excluding the H_2O_2 pathway through the tuning of proton activity, a selectivity switch to H_2O is observed.[1,12]

Cobalt complexes containing non-macrocyclic N_2O_2 salen, salophen, and acen derivatives were recently examined by Stahl and coworkers and found to be competent catalysts for the reduction of O_2 to H_2O_2 in methanol (MeOH) solution with acetic acid (AcOH) as a proton donor and decamethylferrocene (Cp^*_2Fe) as a chemical reductant.[31-33] However, our own report employing a bipyridine-based Co(III)(N_2O_2) complex, initially studied in the context of O_2 binding to the Co(II) state in the presence of pyridine by Thomas and co-workers,[34] **[Co(^{tbu}dhbpy)(py)$_2$][PF$_6$]** (**1**) showed selectivity for the production of H_2O (71±5%) under identical conditions (**Scheme 1**).[35] Here, [^{tbu}dhbpy]$^{2-}$ = 6,6′-di(3,5-di-*tert*-butyl-2-phenolate)-2,2′-bipyridine and py = pyridine. We hypothesized that the Co(III) hydroperoxo resting state was resistant to net protonation and H_2O_2 release due to stronger π-backbonding of the Co center with the bpy backbone relative to other N_2O_2 ligands. The relative decrease in electron density at Co from π-backbonding into the bpy fragment allows the hydroperoxo moiety to donate more π electron density to Co, favoring protonation at the distal O atom relative to the Co center and directing product selectivity towards two equivalents of H_2O.

The study of secondary-sphere effects in O_2 reduction based on hydrogen-bonding motifs is motivated by similar proposed effects in bioinorganic processes, such as the C*c*O O_2 reduction mechanism. In C*c*O, selectivity towards H_2O production is proposed to derive from hydrogen atom transfer from a tyrosine residue to O_2 bound at the heterobimetallic active site, yielding a tyrosyl radical, Fe(IV)(O), and a Cu(II)(OH) species as the result of net O–O bond cleavage.[36] This proposed mechanism has led to the development of a variety of "hangman"-type designs where hydrogen-bonding residues are placed above the active site of catalysis and facilitate O_2 binding, often leading to enhanced rates of O–O bond scission through interaction with the distal O atom of intermediate O_2 adducts.[37-40]

Here we take an alternative approach: hydrogen-bond acceptor –OMe moieties are placed such that they can direct protonation towards the proximal O atom of O_2 fragments bound to Co in a similar fashion to a strategy we have previously used to enhance electrocatalytic CO_2 reduction to formate.[41] We describe the synthesis, characterization, and ORR reactivity of **[Co(^{nPr}bpy)(py)$_2$][PF$_6$]**, **2** (**Figure 1**) in acetonitrile (MeCN) employing benzoic acid derivatives (AH) with varying proton activity, where [^{nPr}bpy]$^{2-}$ = 6,6′-di(3-methoxy-5-*n*-propyl-2-phenolate)-2,2′-bipyridine. Interestingly, the activity of **1** in MeCN is negligible, and instead a comparison with the activity of **2** in MeOH was assessed in parallel. In MeCN and MeOH solution, **2** is selective for H_2O_2 production. Complex **2** also undergoes a change in mechanism in MeCN at high proton activities, with the observed rate showing a dependence on [O_2]. To the best of our knowledge, comparable kinetic control for H_2O_2 with high efficiency has not previously been demonstrated for homogeneous ORR catalysts. Consistent with the proposed kinetic relay effect, although **1** and **2** have identical standard reduction potentials, only **2** exhibits quantifiable activity under otherwise identical conditions.

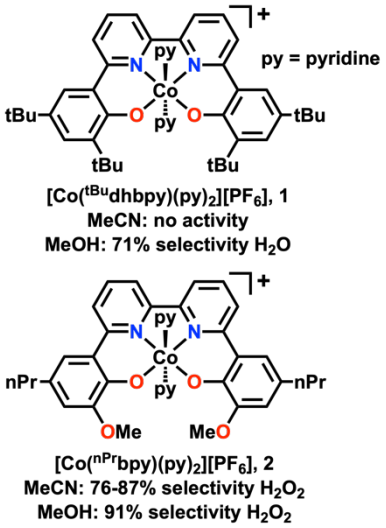

Figure 1. Summary of complexes studied in this work and their ORR selectivity.

Results

Synthesis and Characterization

The synthesis of ^{nPr}**bpy**[H]$_2$ was completed through modification of our previously reported procedure (**Supporting Information**).[41] Isolation of **2** was achieved by adding equivalent amounts of ^{nPr}**bpy**[H]$_2$ and Co(OAc)$_2$•4H$_2$O to a refluxing MeOH solution, followed by the addition of excess pyridine and ammonium hexafluorophosphate. After a 16h reflux, the solution was cooled to room temperature, filtered, and the volatile components were removed under reduced pressure. The isolated solid was recrystallized from a saturated MeOH solution to yield a red-brown diamagnetic crystalline solid. UV-vis spectroscopy in an MeCN solution (**Figure S1**) revealed two absorbance bands with λ_{max} of 253 nm (ε = 2.2 x 10^4 M^{-1} cm^{-1}) and 345 nm (ε = 5.9x10^3 M^{-1} cm^{-1}). Complex **1** was synthesized according to our previously reported procedure.[35]

Initial Reactivity Screening in MeCN

Initial testing for ORR was carried out in MeCN with decamethylferrocene (Cp^*_2Fe) and acids of varying strengths (pK_a) under O_2-saturating conditions. Suitable conditions for the ORR were initially found with benzoic acid (pK_a(MeCN) = 20.4).[42] A structurally homologous series of benzoic acid derivatives (AH) of increasing strength was chosen for subsequent mechanistic study: 2-chlorobenzoic acid (pK_a(MeCN) = 19), 2,4-dichlorobenzoic acid (pK_a(MeCN) = 18.4), and 2,6-dichlorobenzoic acid (pK_a(MeCN) = 17.6) (**Figure 2**).[42] Interestingly, while complex **2** exhibited significant rates of catalysis, complex **1** did not show appreciable activity in MeCN in comparison to the background reaction (**Figures S4-S7**), although this complex is active in MeOH solution with AcOH present (**Figure S8**).[35]

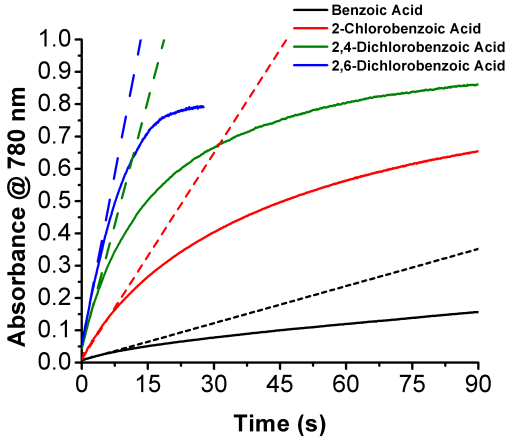

Figure 2. Observed changes in UV-Vis absorbance at 780 nm resulting from catalytic ORR in MeCN. Conditions: 40 uM **2**, 25 mM AH, 1.5 mM Cp^*_2Fe, and 8.1 mM O_2. Dashed lines are extrapolated fits of the initial rates regions.

Electrochemistry in MeCN

Differential pulse voltammetry (DPV) was employed to examine the relevant electrochemical responses of **1** and **2** under Ar and O_2 saturation. For **1**, a single reduction feature is observed with $E_{1/2}$ = –0.76 V vs Fc^+/Fc. Under aprotic conditions, O_2 saturation induces a cathodic shift in the reduction potential of **1** to –0.85 V vs Fc^+/Fc, consistent with O_2 binding (**Figure S9**). Upon the addition of the 25 mM of each AH under Ar saturation, shifts in the reduction potential of **1** of 30-50 mV towards more *negative* potentials are observed (**Figures S10-S13, Table S1**). Addition of 25 mM 1:1 buffers of each $AH:A^-$ pair led to a shift towards negative potentials of ~0.4 V in all cases, consistent with displacement of py from Co(III) and coordination of A^-.

With **2**, a reduction is observed at the same potential as **1,** $E_{1/2}$ = –0.76 V vs Fc^+/Fc. Under aprotic conditions, O_2 saturation causes a positive shift in the reduction potential of **2** to –0.65 V vs Fc^+/Fc, and a second reduction event is observed at –0.94 V vs Fc^+/Fc consistent with O_2 binding and further reduction (**Figure S14**). Upon the addition of each of the four acids under Ar saturation, shifts in the first reduction potential of **2** of 10-20 mV towards more *positive* potentials are observed (**Figures S15-18, Table S1**). Addition of 25 mM 1:1 buffers of each $AH:A^-$ pair again led to a shift in towards negative potentials, although for **2** these amounted to only ~0.1 V in all cases. Interference from the working electrode precludes electrochemical analysis of both **1** and **2** in the presence of O_2 and all of the chosen AH. Although O_2 binding is apparent by CV, competing py loss inhibits the determination of the corresponding second-order rate constant (**Figure S19**).

Selectivity Determination in MeCN

Selectivity for H_2O_2 was determined by a modified spectrophotometric titration method using an acidified $Ti(O)SO_4$ solution (**Figure S20**).[43,44] Briefly, air-saturated solutions of **2** and AH were added to an air-saturated solution of Cp^*_2Fe to give final concentrations of 40 μM catalyst, 25 mM AH, and 0.9-1.5 mM Cp^*_2Fe. The reaction was allowed to run to completion based on the kinetic studies discussed below. Since complex **1** did not exhibit activity in MeCN solution, no reaction selectivity measurements were run (**Figures S4-S7**).

For complex **2**, a range in H_2O_2 selectivity from 76-87% was observed (**Table 1, Figures S21-S28**). We postulate that the shift of selectivity is consistent with the enhancement of the rate of protonation at the proximal O atom in the bound Co(III)-hydroperoxo species relative to the distal O atom. We emphasize that there is no difference in the standard potentials of **1** and **2**, suggesting that the pendent –OMe relay greatly enhances activity and places the system under kinetic control during the ORR. Control experiments indicate that no H_2O_2 disproportionation occurs under catalytic conditions with **2** for any AH (**Figure S29-S32**). Effective overpotentials of 0.33-0.52 V were calculated for the production of H_2O_2 **eq(1)** and 0.81-0.99 V for H_2O **eq(2)** for complexes **1** and **2**, dependent upon AH. We emphasize again that these values are *consistent between the two complexes under otherwise identical conditions and that **1** exhibits no activity in MeCN*. Note that effective overpotential for the electrochemical ORR is defined by the difference between the standard reduction potential that initiates catalysis and the thermodynamic potential of the reaction.[1,32,33,45]

$$O_2 + 2Cp^*_2Fe + 2AH \xrightarrow{Co} H_2O_2 + 2Cp^*_2Fe^+ + 2A^- \quad \textbf{eq(1)}$$

$$O_2 + 4Cp^*_2Fe + 4AH \xrightarrow{Co} 2H_2O + 4Cp^*_2Fe^+ + 4A^- \quad \textbf{eq(2)}$$

Table 1. Summary of selectivity for different acids with complex **2**.

AH (pK_a)	[Co(^{nPr}bpy)(py)$_2$][PF$_6$] H_2O_2 Selectivity (n_{cat})	Background H_2O Selectivity	η_{H2O}[a]	η_{H2O2}[a]
Benzoic Acid (20.7)	81±7% (2.38)	0±4%	0.81	0.33
2-Chlorobenzoic Acid (19)	87±2% (2.26)	0±6%	0.91	0.44
2,4-Dichlorobenzoic Acid (18.4)	81±3% (2.38)	0±2%	0.95	0.47
2,6-Dichlorobenzoic Acid (17.6)	76±3% (2.48)	0±5%	0.99	0.52

Conditions: 40 μM Co, 25 mM AH, air saturation, 0.9 or 1.5 mM Cp*$_2$Fe. Values for n_{cat} are shown in parentheses. Overpotential calculations described in supporting information. [a] - Values for η are consistent between both complexes **1** and **2**.

Spectrochemical Kinetic Studies in MeCN

Kinetic studies were undertaken with Cp*$_2$Fe as a chemical reductant using initial rates. Spectral changes in the visible region were monitored by following the rate of appearance of [Cp*$_2$Fe]$^+$ under O_2 saturation conditions with added AH in MeCN, λ_{max} = 780 nm (ε = 461 M^{-1} cm^{-1} as determined by spectrophotometric titration). Selectivity data was used to determine number of electrons transferred (n_{cat}) for each set of conditions. The catalytic rate law determined for complex **2** conforms to **eq(3)** for benzoic acid and 2-chlorobenzoic acid (**Figures 33-S40**), consistent with that reported for other Co(N_2O_2) complexes in MeOH (**Figure 3**).[31,32,35] From these variable catalyst concentration studies, TOF values were determined with 25 mM AH (**Table 2**).

However, with 2,4-dichlorobenzoic acid (at [O_2] < 4mM) and 2,6-dichlorobenzoic acid, the rate law demonstrates a first-order dependence on [**2**], [HA], and [O_2], with no observed dependence on [Cp*$_2$Fe] (**Figures S41-S48**). We propose that this shift to [O_2] dependence **eq(4)** is consistent with a change in catalyst resting state due to participation of the pendent -OMe relay, *vide infra*.

$$rate = k_{cat}[Co]^1[AH]^1[O_2]^0[Cp^*_2Fe]^0 \qquad \textbf{eq(3)}$$

$$rate = k_{cat}[Co]^1[AH]^1[O_2]^1[Cp^*_2Fe]^0 \qquad \textbf{eq(4)}$$

Determination of Kinetic Isotope Effect in MeCN

To elucidate additional information on **2**, we then evaluated the kinetic isotope effect (KIE, k_H/k_D) with the strongest acid: 2,6-dichlorobenzoic acid. Catalytic reaction rates for both naturally abundant (O–H) and deuterated (O–D) 2,6-dichlorobenzoic acid substrate under variable acid concentration are summarized in **Table 2**. Under these conditions, a KIE value of 2.3±0.1 was obtained for **2** (**Figure 4**).

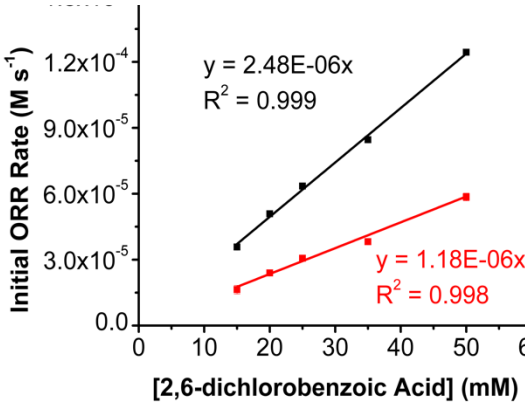

Figure 4. Kinetic isotope effect determination for complex **2**. Black line is with naturally abundant 2,6-dichlorobenzoic acid (O-H). Red line is with isotopically enriched (92%) d_1-2,6-dichlorobenzoic acid (O-D); linear fit procedure with forced zero intercept.

Spectrochemical Kinetic Studies in MeOH

Given that we were unable to assess the activity of **1** directly against that of **2** in MeCN, we quantified the reaction parameters of **2** in MeOH instead, where a complete comparison with **1** is available.[35] With **2** in MeOH, a reduction is observed at $E_{1/2}$ = –0.74 V vs Fc$^+$/Fc by DPV. Upon the addition of AcOH under Ar

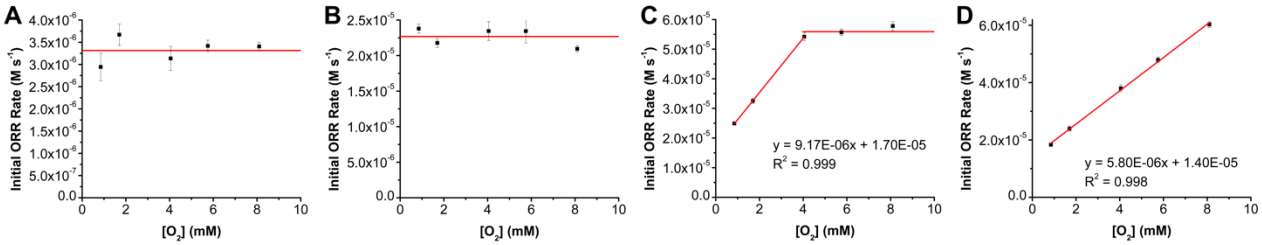

Figure 3. Variable O_2 concentration studies with 40 μM **2**, 1.5 mM Cp*$_2$Fe, and 25 mM AH. (**A**) Benzoic acid; (**B**) 2-chlorobenzoic acid; (**C**) 2,4-dichlorobenzoic acid; (**D**) 2,6-dichlorobenzoic acid.

saturation, shifts in the first reduction potential of **2** of 50 mV towards more positive potentials are observed (**Figure S49, Table S2**).

The catalytic rate law determined for complex **2** in MeOH with added AcOH conforms to **eq(5)** (**Figures S50-S53**), in contrast with that reported for other Co(N_2O_2) complexes in MeOH.[31,32,35] For comparison, complex **1** was previously determined to conform to **eq(3)**, producing H_2O with 71±5% efficiency.[35] Under otherwise identical conditions, complex **2** instead produces H_2O_2 with 91±5% efficiency (**Figure S54**). The dependence of the catalytic rate on [Cp^*_2Fe] suggests that the redox-dependent O_2 binding step has become rate determining under these conditions. Consistent with the pendent relay enhancing effective proton activity, control testing without AcOH present shows that the apparent zero-order dependence of [AcOH] on the observed rate is the result of saturation kinetics at low concentrations (**Figure S51**).

$$rate = k_{cat}[Co]^1[AH]^0[O_2]^1[Cp^*_2Fe]^1 \qquad \textbf{eq(5)}$$

Electron Paramagnetic Resonance Spectroscopy

In order to better understand the nature of the chemically accessible species and reaction intermediates, EPR spectroscopy was performed on frozen solutions of **[Co(^{tBu}dhbpy)]^0** (**3**) and **[Co(^{nPr}bpy)]^0** (**4**) prepared aerobically in CH_2Cl_2 in the presence and absence of excess pyridine. We note that CH_2Cl_2 was used to circumvent solubility limitations of the neutral Co(II) species and provide a non-coordinating solvent environment. The X-band EPR spectrum of **[Co(^{tBu}dhbpy)]^0 3** at 30 K exhibits a narrow, rhombic signal spanning approximately 42 mT (**Figure 5A**). Hyperfine coupling to the ^{59}Co nucleus is evident on the low- and center-field turning points, and the spectrum is adequately simulated[46] with g_x = 2.019, g_y = 2.110, g_z = 1.990 and $A_x(^{59}Co)$ = 18 MHz, $A_y(^{59}Co)$ = 55 MHz, and $A_z(^{59}Co)$ = 49 MHz. The signal intensity is consistent with near-quantitative population of the S = ½ species, and in the absence of exogenous base, no change is observed upon exposure to O_2 (**Figure S55**). We assign this species to a low-spin, pseudo-octahedral Co(II) species with weak axial ligation, likely residual MeOH or water from the sample preparation procedure, which would give rise to the low g-tensor anisotropy and hyperfine coupling observed; four-coordinate square planar and five-coordinate square-pyramidal Co(II) species, such as those observed in cobalt porphyrins, corrins, Schiff-base complexes, cobaloximes, and related compounds generally show large g-tensor anisotropy, with low-field g-values between 2.3 and 2.2, respectively.[47-51] In the presence of excess pyridine, the EPR spectrum of aerated **3** changes slightly, retaining near-quantitative intensity and exhibiting features that are consistent with the formation of a six-coordinate Co^{III}-$O_2^{\bullet-}$ species,[47,51-55] with g_x = 2.017, g_y = 2.095, g_z = 1.990 and $A_x(^{59}Co)$ = 24 MHz, $A_y(^{59}Co)$ = 45 MHz, and $A_z(^{59}Co)$ = 28 MHz. Extended exposure of **3** to O_2 in the presence of pyridine leads to a >50% decrease in spin concentration. These results can be rationalized by the formation of the bridging Co(III)–O_2^{2-}–Co(III) species, as noted previously for Co(salen) compounds.[32] Addition of 2,6-dichlorobenzoic acid results in only EPR-silent species, which suggests formation of a Co(III) – OOH species.

In contrast to the near-quantitative EPR signals seen for solutions of **3**, only trace amounts of EPR-active species are observed for **[Co(^{nPr}bpy)]^0 4** in the absence of excess base. The electronic structure of **4** differs only slightly from that of **3** but the substantial decrease in signal suggests a strong propensity for dimerization in the divalent state (**Figure S56**). Consistent with this hypothesis, the addition of excess pyridine restores signal intensity, with formation of a new species that closely resembles that of the **3**(py)O_2 adduct is observed for **4**(py)O_2, with g_x = 2.017, g_y = 2.100, g_z = 1.990 and $A_x(^{59}Co)$ = 25 MHz, $A_y(^{59}Co)$ = 53 MHz, and $A_z(^{59}Co)$ = 32 MHz (**Figure 5B**). Addition of excess O_2 quenches the **4**(py)O_2 signal almost fully, again indicating formation of a bridging peroxide dimer (**Figure S58**), and no EPR-active species are observed in the presence of 2,6-dichlorobenzoic acid. In both cases, the EPR spectral features support formation of a Co(III)-$O_2^{\bullet-}$ species, with the relative intensity differences between **3**(py)O_2 and **4**(py)O_2 suggesting more rapid and quantitative O_2 binding to **4**.

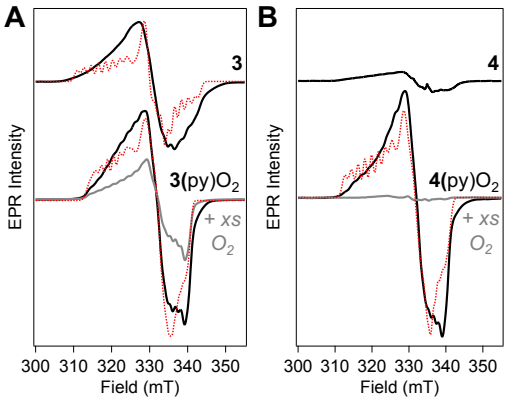

Figure 5. CW X-band EPR spectra (T = 30 K; $P_{\mu w}$ = 2 mW) of 250 µM (**A**) **3** and (**B**) **4** in the absence and presence of excess py, as indicated. Samples were prepared aerobically in CH_2Cl_2. Simulations overlaid in red dashed lines were generated with the parameters indicated in the text including isotropic A-strain of 10 MHz and 1 mT line broadening. The simulation for **3**(py)O_2 used an anisotropic A-strain of 15, 15, 6.3 MHz in addition to 1 mT isotropic line broadening.

DFT Calculations

To reconcile our mechanistic observations in MeCN, we examined the initial steps of the reaction computationally by DFT methods. Consistent with our observations[35] and those of Thomas and co-workers,[34] these predict that in the absence of reductant, the predominant Co(III) species should be a bis-py adduct, $[Co(^{nPr}dhbpy)(py)_2]^+$ S = 0. Further, upon one-electron reduction, the dissociation of a single equivalent of py to generate a five-coordinate coordination mode is exergonic by 7.8 kcal/mol, $[Co(^{nPr}dhbpy)(py)]^0$ S = ½ (**Figure 6**). The exchange of the axial py with an equivalent of MeCN to generate $[Co(^{nPr}dhbpy)(MeCN)]^0$ S = ½ is favored slightly under reaction conditions.

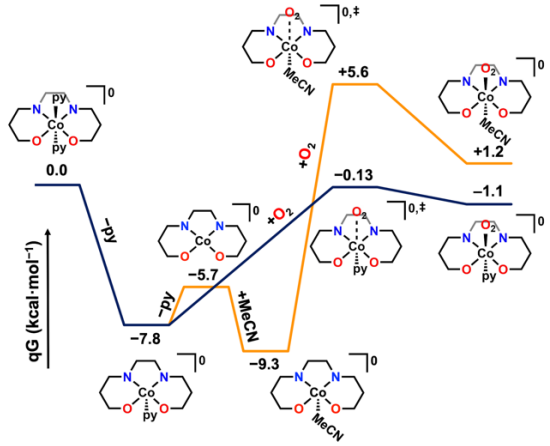

Figure 6. Reaction profile predicted by DFT methods for O_2 binding by complex **2** upon one-electron reduction; all species are in the S = ½ manifold.

Although the formation of the five-coordinate solvento species is favored slightly, the mono py adduct presents a barrier for O_2 binding of 7.7 kcal/mol, lower than that predicted for the solvento species, 14.9 kcal/mol, in a S = ½ spin configuration (**Figure 6**). The O_2 binding reaction is endergonic for both axial ligands, but again py (+6.8 kcal/mol) if more favorable than MeCN (+10.6 kcal/mol). Overall, these key differences place the py-assisted pathway as the lowest energy and thermodynamically favorable. Comparable quartet manifolds did not result in stable O_2 adducts and no barrier for O_2 binding could be located without an axial ligand present. EPR properties for possible resting species were also calculated (**Table S3**). Good agreement between the calculated and experimentally observed *g*- and A-tensors was obtained for the **4**(py)(O_2) species, with g_{calc} = [1.985, 2.003, 2.047] and $A_{calc}(^{59}Co)$ = [22, 29, 77] MHz.

Discussion

These data demonstrate that complex **1** is inactive for ORR under all examined conditions in MeCN, while **2** is 76-87% selective for H_2O_2. This is noteworthy, *given that there is no quantifiable difference in their standard reduction potentials*. To assess if the minimal activity of complex **1** in MeCN was the result of steric effects, an additional control complex was prepared. For this new catalyst, $[Co(^{p\text{-}tBu}dhbpy)(py)_2][PF_6]$ **5** (where $^{p\text{-}tBu}$dhbpy = 2,2'-([2,2'-bipyridine]-6,6'-diyl)bis(4-(tert-butyl)phenol)), an H atom was substituted adjacent to the Co-coordinated O atom of the ligand, where complexes **1** and **2** have *tert*-butyl and methoxy functional groups, respectively. Under Ar saturation in MeCN, complex **5** has a catalytically relevant $E_{1/2}$ = −0.78 V vs Fc^+/Fc, which is only 20 mV more negative than both **1** and **2**. Under catalytic conditions in MeCN with 2,6-dichlorobenzoic acid as the proton donor, complex **5** has a selectivity for H_2O_2 of only 21±5% (79±5% selectivity for H_2O). In addition to suggesting a steric inhibition for complex **1**, the observed selectivity for complex **5** is consistent with a secondary-sphere effect altering mechanism,[41,56-59] since it is expected that for catalysts within the same family, activity and selectivity will scale with overpotential.

Table 2. Summary of turnover frequencies (TOF), and second- and third-order rate constants for different acids with complex **2** in MeCN.

AH (pK_a)	TOF (s^{-1})	Second-Order Rate Constant ($M^{-1}s^{-1}$)[a]	Third-Order Rate Constant ($M^{-2}s^{-1}$)[b]
Benzoic Acid (20.7)	1.0 x 10^{-1}±0.1 x 10^{-1} s^{-1}	4.1	n/a
2-Chlorobenzoic Acid (19)	3.3 x 10^{-1}±0.1 x 10^{-1} s^{-1}	13	n/a
2,4-Dichlorobenzoic Acid (18.4)	7.8 x 10^{-1}±0.1 x 10^{-1} s^{-1}	n/a	3.8 x 10^3
2,6-Dichlorobenzoic Acid (17.6)	1.9±0.1 s^{-1} (O–H) 0.94±0.05 s^{-1} (O–D)	n/a	9.2 x 10^3

Conditions: variable [Co], 25 mM AH, O_2 saturation, 1.5 mM Cp^*_2Fe. The deuterated 2,6-dichlorobenzoic acid substrate was prepared with 92% O–D substitution. [a] – determined using Co and AH; [b] – determined using Co, AH, and O_2, where possible.

We propose the overall enhanced kinetic selectivity for H_2O_2 observed for **2** under all conditions is the result of the alkyl ether pendent relay enhancing proton transfer to the proximal O atom of a Co(III)–(OOH) intermediate, accelerating H_2O_2 dissociation (**Figure 7**). With benzoic acid and 2-chlorobenzoic acid, this protonation step (**Figure 8, Step C**) remains rate-determining and the catalytic rate law shows no $[O_2]$ dependence but is dependent on [Co] and [AH], implying that ***iii*** is the resting state of the catalytic cycle, as has been proposed previously for salen- and salophen-based complexes.[31-33]

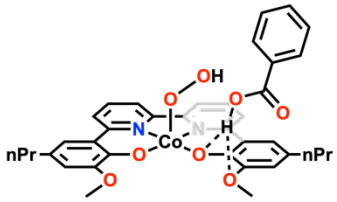

Figure 7. Proposed pendent relay interaction relevant to the kinetic selectivity of ORR mediated by complex **2**.

Interestingly, additional mechanistic consequences of the pendent relay become apparent with the stronger acids, 2,4-dichlorobenzoic acid and 2,6-dichlorobenzoic acid. Not only is the kinetic selectivity for H_2O_2 retained, but with the stronger acids 2,4-dichlorobenzoic acid and 2,6-dichlorobenzoic acid as the proton source, the rate becomes dependent on $[O_2]$, as well as [Co] and [AH]. Based on these observations, we propose that the resting state of catalysis for **2** (**Figure 8**) with the stronger acids shifts to $[Co(II)(^{nPr}dhbpy)(py)(O_2)]^0$ (***ii***). Initially, an equilibrium reaction between ***i*** and O_2 occurs, which we propose is followed by rate-determining proton-transfer reaction (**Step B**) to produce a $[Co(III)–OOH]^+$ species. Under reaction conditions, it is likely that subsequent reduction occurs rapidly. From species (***iii***), the pendent –OMe relay again directs a proton equivalent towards the proximal O atom of the hydroperoxide ligand, which is again the selectivity-determining step of the reaction. The protonation of Co(III)-OOH to generate a bound H_2O_2 adduct precedes net dissociation of H_2O_2 and binding of py to regenerate ***i*** (**Figures 7 and 8**).

Evidence of proton transfer involving the relay being the rate-determining step with the stronger acids is directly obtained from the KIE data: for complex **2**, a KIE of 2.3±0.1 is observed (**Figure 8**).[60-62] The absence of catalytic rate dependence on the concentration of the reductant for stronger acids suggests that this proton transfer is decoupled from electron transfer, eliminating the possibility of a concerted PCET step under these conditions.

We note that the formation of bridging $Co(III)–O_2^{2-}–Co(III)$ species cannot be excluded, based on the observed shift to diamagnetic species in the EPR under O_2 saturation. However, the observation of EPR signals characteristic of $Co(III)\text{-}O_2^{\bullet-}$ species under low $[O_2]$ exposures supports the intermediacy of monomeric species[63-66] and we postulate that a dynamic off-cycle equilibrium exists between monomer and dimer. Stahl and co-workers have previously demonstrated that at the low [Co] used under catalytic conditions, monomer speciation is generally >95%.[32] Consistent with this, DFT calculations on a probable dimer structure (**Figure S59**) suggest that its formation from the O_2 adduct (***ii***) and $[Co(II)(^{nPr}dhbpy)(py)]^0$ is endergonic by 6.4 kcal/mol under catalytic conditions.

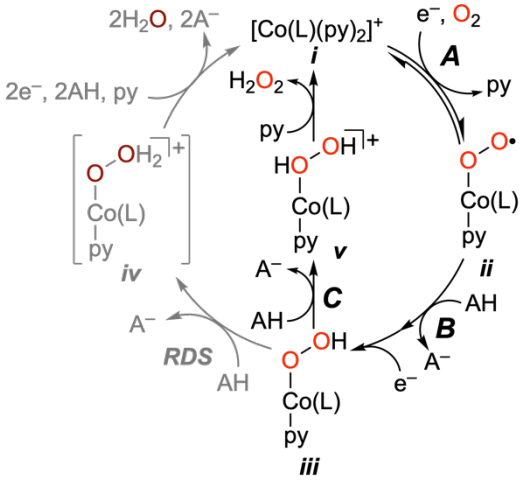

Figure 8. General proposed ORR mechanism for complex **2** in MeCN.

Comparing the data obtained in MeOH for complex **2** with the effective overpotentials, selectivity, and rates of our previous report also leads to a few observations. As mentioned above, complex **1** produces H_2O with 71±5% selectivity in MeOH solution with AcOH, whereas 91±5% selectivity is achieved for H_2O_2 during ORR mediated by **2**.[35] However, the near quantitative kinetic selectivity for complex **2** in protic solvent cannot be exclusively attributed to the inclusion of the pendent –OMe relay. The steric profile at Co also appears to play an important role for ORR selectivity in MeOH; control experiments with complex **5**, under otherwise identical conditions show 78±7% selectivity for H_2O_2. Overall, for complex **2** the shift to a rate dependence on [Co], $[O_2]$, and $[Cp^*_2Fe]$ and the saturation of the observed rate at low [AcOH] suggests that in MeOH the rate-determining step has shifted to O_2 binding following one-electron reduction (**Figure 8, Step A**).

We emphasize that DPV experiments described above with 1:1 buffered conditions of $HA:A^-$ indicate coordination by benzoate anions in the Co(III) oxidation state, which has previously been shown to

alter reaction mechanism in other systems for ORR.[67] This precludes kinetic measurements under buffered conditions and suggests that over time, as the reaction proceeds to completion, the resting state of the catalyst and the observed rate are both likely to change as benzoate anion concentrations increase and change the catalyst standard potential. Since the homoconjugation values of the benzoic acid derivatives are known in MeCN, it is possible to account for their thermodynamic contribution[68] to the estimated standard potential of the reaction (See SI). The resultant effective overpotentials should be regarded as a lower-limit estimate for this value, given that we were unable to measure buffered conditions.

Conclusions

We have reported a new Co(III)(N_2O_2) complex bearing pendent –OMe relays for the ORR. Mechanistic studies reveal a change in mechanism at high proton activities for this complex, with the reaction shifting to [O_2] dependence. This change is consistent with a shift in the rate determining step to protonation of a Co(III)($O_2^{\bullet-}$) (***ii***) intermediate (**Figure 8**), decoupling it from electron transfer. This assignment is supported by KIE studies and the absence of a concentration dependence on the reductant.

For ORR mediated by **2**, selectivity for H_2O_2 (76–81% H_2O_2) is observed in MeCN with TOF = 1.0 x 10^{-1} to 1.5 s^{-1} at estimated effective overpotentials of 330-520 mV. In contrast to this, complex **1** is inactive in MeCN under otherwise identical conditions, which control experiments with complex **5** suggest can be attributed to steric effects. Since all three complexes have near identical standard reduction potentials (which defines the effective reaction overpotential as almost identical for all three systems[1,32,33,45]), these results are consistent with a breaking of the expected reaction scaling relationship through secondary-sphere effects involving the alkyl ether groups.[41,56-59] For complex **2**, these relays place the reaction under kinetic control, producing H_2O_2 as the primary reaction product. Control complex **5**, where the pendent relay has been replaced with an H atom, instead exhibits a selectivity for H_2O of 79±5% under the same conditions in MeCN. Interestingly, in MeOH solution with AcOH, **2** shows near quantitative selectivity toward H_2O_2 (91±5%) and **5** shifts to a H_2O_2 selectivity of 78±7%, suggesting that in the protic solvent the steric profile of the ligand alters reaction selectivity as well. This demonstrates a more balanced relationship between the role of the pendent relay and steric effects in the protonation of the hydroperoxo intermediate during the ORR in MeOH.

This work helps broaden the understanding of the ORR utilizing non-macrocyclic Co complexes and has the potential to lead to active catalysts for the ORR to either H_2O_2 or H_2O with high selectivity and activity. Further studies on the underlying non-covalent solvent effects, mechanistic dependence on proton activity, and the tunability of axial ligand effects on O_2 binding are currently underway.

Associated Content

Supporting Information can be found at XXX. SI includes synthesis, characterization, electrochemistry, additional EPR spectra and simulations, and descriptions of experimental methods. Crystallographic data available under CCDC: 2084949.

Author Information

Corresponding Author

machan@virginia.edu

ORCID

CWM: 0000-0002-5282-1138

AWN: 0000-0002-8480-5118

YJG: 0000-0002-6391-4286

ENC: 0000-0002-0568-3600

DAD: 0000-0003-0939-3309

HSS: 0000-0003-0793-4650

JMD: 0000-0002-3601-9710

Author Contributions

The manuscript was written through the contribution of all authors.

Funding Sources

We thank the University of Virginia for generous funding and infrastructural support. A.W.N., E.N.C., and C.W.M. acknowledge N.S.F. CHE-2102156 and ACS PRF 61430-ND3 for support. H.S.S. and Y.J.G. acknowledge the N.I.H. R35-GM128852 for support.

References

1. Pegis, M. L.; Wise, C. F.; Martin, D. J.; Mayer, J. M., Oxygen Reduction by Homogeneous Molecular Catalysts and Electrocatalysts. *Chem. Rev.* **2018,** *118*, 2340-2391.

2. Machan, C. W., Advances in the Molecular Catalysis of Dioxygen Reduction. *ACS Catal.* **2020,** *10*, 2640-2655.

3. Steele, B. C. H.; Heinzel, A., Materials for fuel-cell technologies. In *Materials for Sustainable Energy: A Collection of Peer-Reviewed Research and Review Articles from Nature Publishing Group*, Dusastre, V., Ed. World Scientific: 2011; pp 224-231.

4. Borup, R.; Meyers, J.; Pivovar, B.; Kim, Y. S.; Mukundan, R.; Garland, N.; Myers, D.; Wilson, M.; Garzon, F.; Wood, D., Scientific aspects of polymer electrolyte fuel cell durability and degradation. *Chem. Rev.* **2007,** *107*, 3904-3951.

5. Collman, J. P.; Boulatov, R.; Sunderland, C. J.; Fu, L., Functional analogues of cytochrome c oxidase, myoglobin, and hemoglobin. *Chem. Rev.* **2004,** *104*, 561-588.

6. He, Q.; Mugadza, T.; Hwang, G.; Nyokong, T., Mechanisms of Electrocatalysis of Oxygen Reduction by Metal Porphyrins in Trifluoromethane Sulfonic Acid Solution *Int. J. Electrochem. Sci.* **2012,** *7*, 7045 - 7064.

7. Chan, R. J.; Su, Y. O.; Kuwana, T., Electrocatalysis of oxygen reduction. 5. oxygen to hydrogen peroxide conversion by cobalt (II) tetrakis (N-methyl-4-pyridyl) porphyrin. *Inorg. Chem.* **1985,** *24*, 3777-3784.

8. Sazou, D.; Araullo-McAdams, C.; Han, B.; Franzen, M.; Kadish, K. M., The use of an electrogenerated cobalt (I) porphyrin for the homogeneous catalytic reduction of dioxygen in dimethylformamide. Reactions of [(TMpyP) CoII] 4+ and [(TMpyP) CoI] 3+ where TMpyP= meso-tetrakis (1-methylpyridinium-4-yl) porphyrin. *J. Am. Chem. Soc.* **1990,** *112*, 7879-7886.

9. D'Souza, F.; Deviprasad, R.; Hsieh, Y.-Y., Synthesis and studies on the electrocatalytic reduction of molecular oxygen by non-planar cobalt (II) tetrakis-(N-methyl pyridyl)-β-octabromoporphyrin. *J. Electroanal. Chem.* **1996,** *411*, 167-171.

10. D'Souza, F.; Hsieh, Y.-Y.; Deviprasad, G., Electrocatalytic reduction of molecular oxygen using non-planar cobalt tetrakis-(4-sulfonatophenyl)-β-octabromoporphyrin. *J. Electroanal. Chem.* **1997,** *426*, 17-21.

11. Trojanek, A.; Langmaier, J.; Kvapilová, H.; Záliš, S.; Samec, Z. k., Inhibitory effect of water on the oxygen reduction catalyzed by cobalt (II) tetraphenylporphyrin. *J. Phys. Chem. A* **2014,** *118*, 2018-2028.

12. Wang, Y.-H.; Schneider, P. E.; Goldsmith, Z. K.; Mondal, B.; Hammes-Schiffer, S.; Stahl, S. S., Brønsted Acid Scaling Relationships Enable Control Over Product Selectivity from O2 Reduction with a Mononuclear Cobalt Porphyrin Catalyst. *ACS Cent. Sci.* **2019,** *5*, 1024-1034.

13. Fukuzumi, S.; Mochizuki, S.; Tanaka, T., Efficient reduction of dioxygen with ferrocene derivatives, catalyzed by metalloporphyrins in the presence of perchloric acid. *Inorg. Chem.* **1989,** *28*, 2459-2465.

14. Fukuzumi, S.; Mochizuki, S.; Tanaka, T., Metalloporphyrin-catalyzed reduction of dioxygen by ferrocene derivatives. *Chem. Lett.* **1989,** *18*, 27-30.

15. Fukuzumi, S.; Okamoto, K.; Gros, C. P.; Guilard, R., Mechanism of four-electron reduction of dioxygen to water by ferrocene derivatives in the presence of perchloric acid in benzonitrile, catalyzed by cofacial dicobalt porphyrins. *J. Am. Chem. Soc.* **2004,** *126*, 10441-10449.

16. Oldacre, A. N.; Friedman, A. E.; Cook, T. R., A self-assembled cofacial cobalt porphyrin prism for oxygen reduction catalysis. *J. Am. Chem. Soc.* **2017,** *139*, 1424-1427.

17. Kadish, K. M.; Shen, J.; Frémond, L.; Chen, P.; El Ojaimi, M.; Chkounda, M.; Gros, C. P.; Barbe, J.-M.; Ohkubo, K.; Fukuzumi, S., Clarification of the oxidation state of cobalt corroles in heterogeneous and homogeneous catalytic reduction of dioxygen. *Inorg. Chem.* **2008,** *47*, 6726-6737.

18. Meng, J.; Lei, H.; Li, X.; Zhang, W.; Cao, R., The Trans Axial Ligand Effect on Oxygen Reduction. Immobilization Method May Weaken Catalyst Design for Electrocatalytic Performance. *J. Phys. Chem. C* **2020,** *124*, 16324-16331.

19. Honda, T.; Kojima, T.; Fukuzumi, S., Proton-Coupled Electron-Transfer Reduction of Dioxygen Catalyzed by a Saddle-Distorted Cobalt Phthalocyanine. *J. Am. Chem. Soc.* **2012,** *134*, 4196-4206.

20. Kobayashi, N.; Nevin, W. A., Electrocatalytic Reduction of Oxygen Using Water-Soluble Iron and Cobalt Phthalocyanines and Porphyrins. *Appl. Organomet. Chem.* **1996,** *10*, 579-590.

21. Kobayashi, N.; Nishiyama, Y., Catalytic electroreduction of molecular oxygen using iron or cobalt 4, 4', 4", 4'"-tetracarboxyphthalocyanine. *J. Phys. Chem.* **1985,** *89*, 1167-1170.

22. Mho, S. i.; Ortiz, B.; Doddapaneni, N.; Park, S. M., Electrochemical and Spectroelectrochemical Studies on Metallophthalocyanine-Oxygen Interactions in Nonaqueous Solutions. *J. Electrochem. Soc.* **1995,** *142*, 1047.

23. Patir, I. H., Fluorinated-cobalt phthalocyanine catalyzed oxygen reduction at liquid/liquid interfaces. *Electrochim. Acta* **2013,** *87*, 788-793.

24. Mase, K.; Ohkubo, K.; Fukuzumi, S., Efficient Two-Electron Reduction of Dioxygen to Hydrogen Peroxide with One-Electron Reductants with a Small Overpotential Catalyzed by a Cobalt Chlorin Complex. *J. Am. Chem. Soc.* **2013,** *135*, 2800-2808.

25. Mase, K.; Ohkubo, K.; Fukuzumi, S., Much Enhanced Catalytic Reactivity of Cobalt Chlorin Derivatives on Two-Electron Reduction of Dioxygen to Produce Hydrogen Peroxide. *Inorg. Chem.* **2015,** *54*, 1808-1815.

26. Geiger, T.; Anson, F. C., Homogeneous catalysis of the electrochemical reduction of dioxygen by a macrocyclic cobalt (III) complex. *J. Am. Chem. Soc.* **1981,** *103*, 7489-7496.

27. Kang, C.; Anson, F. C., Effects of Coordination to a Macrocyclic Cobalt Complex on the Electrochemistry of Dioxygen, Superoxide, and Hydroperoxide. *Inorg. Chem.* **1995,** *34*, 2771-2780.

28. Wong, C.-L.; Switzer, J. A.; Balakrishnan, K.; Endicott, J. F., Oxidation-reduction reactions of complexes with macrocyclic ligands. Oxygen uptake kinetics, equilibriums and intermediates in aqueous CoII (N4) systems. *J. Am. Chem. Soc.* **1980,** *102*, 5511-5518.

29. Wong, C.-L.; Endicott, J. F., Oxidation-reduction reactions of complexes with macrocyclic ligands. Role of intermediates in reactions of. mu.-peroxo-dicobalt complexes. *Inorg. Chem.* **1981,** *20*, 2233-2239.

30. Kumar, K.; Endicott, J. F., Oxidation-reduction reactions of complexes with macrocyclic ligands. Electron-transfer reactivity of a 1: 1 cobalt (II)-dioxygen adduct. *Inorg. Chem.* **1984,** *23*, 2447-2452.

31. Wang, Y.-H.; Mondal, B.; Stahl, S. S., Molecular Cobalt Catalysts for O2 Reduction to H2O2: Benchmarking Catalyst Performance via Rate–Overpotential Correlations. *ACS Catal.* **2020,** *10*, 12031-12039.

32. Wang, Y.-H.; Goldsmith, Z. K.; Schneider, P. E.; Anson, C. W.; Gerken, J. B.; Ghosh, S.; Hammes-Schiffer, S.; Stahl, S. S., Kinetic and Mechanistic Characterization of Low-Overpotential, H2O2-Selective Reduction of O2 Catalyzed by N2O2-Ligated Cobalt Complexes. *J. Am. Chem. Soc.* **2018,** *140*, 10890-10899.

33. Wang, Y.-H.; Pegis, M. L.; Mayer, J. M.; Stahl, S. S., Molecular Cobalt Catalysts for O2 Reduction: Low-Overpotential Production of H2O2 and Comparison with Iron-Based Catalysts. *J. Am. Chem. Soc.* **2017,** *139*, 16458-16461.

34. Arora, H.; Philouze, C.; Jarjayes, O.; Thomas, F., CoII, NiII, CuII and ZnII complexes of a bipyridine bis-phenol conjugate: Generation and properties of coordinated radical species. *Dalton Trans.* **2010,** *39*, 10088–10098.

35. Nichols, A. W.; Kuehner, J. S.; Huffman, B. L.; Miedaner, P. R.; Dickie, D. A.; Machan, C. W., Reduction of dioxygen to water by a Co(N2O2) complex with a 2,2′-bipyridine backbone. *Chem. Commun.* **2021,** *57*, 516-519.

36. Yoshikawa, S.; Shimada, A., Reaction mechanism of cytochrome c oxidase. *Chem. Rev.* **2015,** *115*, 1936-1989.
37. Rosenthal, J.; Nocera, D. G., Role of proton-coupled electron transfer in O–O bond activation. *Acc. Chem. Res.* **2007,** *40*, 543-553.
38. Baran, J. D.; Grönbeck, H.; Hellman, A., Analysis of Porphyrines as Catalysts for Electrochemical Reduction of O2 and Oxidation of H2O. *J. Am. Chem. Soc.* **2014,** *136*, 1320-1326.
39. Ohta, T.; Nagaraju, P.; Liu, J.-G.; Ogura, T.; Naruta, Y., The secondary coordination sphere and axial ligand effects on oxygen reduction reaction by iron porphyrins: a DFT computational study. *J. Biol. Inorg. Chem.* **2016,** *21*, 745-755.
40. Chng, L. L.; Chang, C. J.; Nocera, D. G., Catalytic O–O Activation Chemistry Mediated by Iron Hangman Porphyrins with a Wide Range of Proton-Donating Abilities. *Org. Lett.* **2003,** *5*, 2421-2424.
41. Nichols, A. W.; Hooe, S. L.; Kuehner, J. S.; Dickie, D. A.; Machan, C. W., Electrocatalytic CO2 Reduction to Formate with Molecular Fe(III) Complexes Containing Pendent Proton Relays. *Inorg. Chem.* **2020,** *59*, 5854-5864.
42. Izutsu, K., *Acid-base dissociation constants in dipolar aprotic solvents*. Blackwell Scientific Publications: Oxford; Boston : Brookline Village, Mass, 1990; Vol. 35.
43. Anson, C. W.; Stahl, S. S., Cooperative Electrocatalytic O2 Reduction Involving Co(salophen) with p-Hydroquinone as an Electron–Proton Transfer Mediator. *J. Am. Chem. Soc.* **2017,** *139*, 18472-18475.
44. Hooe, S. L.; Machan, C. W., Dioxygen Reduction to Hydrogen Peroxide by a Molecular Mn Complex: Mechanistic Divergence between Homogeneous and Heterogeneous Reductants. *J. Am. Chem. Soc.* **2019,** *141*, 4379-4387.
45. Pegis, M. L.; McKeown, B. A.; Kumar, N.; Lang, K.; Wasylenko, D. J.; Zhang, X. P.; Raugei, S.; Mayer, J. M., Homogenous Electrocatalytic Oxygen Reduction Rates Correlate with Reaction Overpotential in Acidic Organic Solutions. *ACS Cent. Sci.* **2016,** *2*, 850-856.
46. Stoll, S.; Schweiger, A., EasySpin, a comprehensive software package for spectral simulation and analysis in EPR. *J. Mag. Res.* **2006,** *178*, 42-55.
47. Joerin, E.; Schweiger, A.; Guenthard, H. H., Single-crystal EPR of the oxygen-17-enriched dioxygen adduct of vitamin B12r: reversible oxygen bonding, electronic and geometric structure and molecular dynamics. *J. Am. Chem. Soc.* **1983,** *105*, 4277-4286.
48. Van Doorslaer, S.; Jeschke, G.; Epel, B.; Goldfarb, D.; Eichel, R.-A.; Kräutler, B.; Schweiger, A., Axial Solvent Coordination in "Base-Off" Cob(II)alamin and Related Co(II)-Corrinates Revealed by 2D-EPR. *J. Am. Chem. Soc.* **2003,** *125*, 5915-5927.
49. Collman, J. P.; Berg, K. E.; Sunderland, C. J.; Aukauloo, A.; Vance, M. A.; Solomon, E. I., Distal Metal Effects in Cobalt Porphyrins Related to CcO. *Inorg. Chem.* **2002,** *41*, 6583-6596.
50. Diemente, D.; Hoffman, B. M.; Basolo, F., Electron spin resonance studies of 1:1 cobalt–oxygen adducts. *J. Chem. Soc. D* **1970**, 467-468.
51. Niklas, J.; Mardis, K. L.; Rakhimov, R. R.; Mulfort, K. L.; Tiede, D. M.; Poluektov, O. G., The Hydrogen Catalyst Cobaloxime: A Multifrequency EPR and DFT Study of Cobaloxime's Electronic Structure. *J. Phys. Chem. B* **2012,** *116*, 2943-2957.
52. Ikeda-Saito, M.; Yamamoto, H.; Imai, K.; Kayne, F. J.; Yonetani, T., Studies on cobalt myoglobins and hemoglobins. Preparation of isolated chains containing cobaltous protoporphyrin IX and characterization of their equilibrium and kinetic properties of oxygenation and EPR spectra. *J. Biol. Chem.* **1977,** *252*, 620-624.
53. Attanasio, D.; Dessy, G.; Fares, V.; Pennesi, G., Synthesis, structural, and E.S.R. studies of some low-spin Co(II) complexes with tetradentate N2S2 and N2Se2 Schiff-bases. *Mol. Phys.* **1980,** *40*, 269-283.
54. Ramdhanie, B.; Telser, J.; Caneschi, A.; Zakharov, L. N.; Rheingold, A. L.; Goldberg, D. P., An Example of O2 Binding in a Cobalt(II) Corrole System and High-Valent Cobalt–Cyano and Cobalt–Alkynyl Complexes. *J. Am. Chem. Soc.* **2004,** *126*, 2515-2525.
55. Hoffman, B. M.; Diemente, D. L.; Basolo, F., Electron paramagnetic resonance studies of some cobalt(II) Schiff base compounds and their monomeric oxygen adducts. *J. Am. Chem. Soc.* **1970,** *92*, 61-65.
56. Nichols, A. W.; Machan, C. W., Secondary-Sphere Effects in Molecular Electrocatalytic CO2 Reduction. *Front. Chem.* **2019,** *7*, https://doi.org/10.3389/fchem.2019.00397.
57. Williams, C. K.; Lashgari, A.; Tomb, J. A.; Chai, J.; Jiang, J. J., Atropisomeric Effects of Second Coordination Spheres on Electrocatalytic CO2 Reduction. *ChemCatChem* **2020,** *12*, 4886-4892.
58. Nichols, Eva M.; Derrick, J. S.; Nistanaki, S. K.; Smith, P. T.; Chang, C. J., Positional effects of second-sphere amide pendants on electrochemical CO2 reduction catalyzed by iron porphyrins. *Chem. Sci.* **2018,** *9*, 2952-2960.
59. Passard, G.; Dogutan, D. K.; Qiu, M.; Costentin, C.; Nocera, D. G., Oxygen reduction reaction promoted by manganese porphyrins. *ACS Catal.* **2018,** *8*, 8671-8679.
60. Savéant, J.-M., Proton Relays in Molecular Catalysis of Electrochemical Reactions: Origin and Limitations of the Boosting Effect. *Angew. Chem., Int. Ed.* **2019,** *58*, 2125-2128.
61. Hammes-Schiffer, S.; Iordanova, N., Theoretical studies of proton-coupled electron transfer reactions. *Biochim. Biophys. Acta Bioenerg.* **2004,** *1655*, 29-36.
62. Iordanova, N.; Decornez, H.; Hammes-Schiffer, S., Theoretical study of electron, proton, and proton-coupled electron transfer in iron bi-imidazoline complexes. *J. Am. Chem. Soc.* **2001,** *123*, 3723-3733.
63. Nguyen, A. I.; Hadt, R. G.; Solomon, E. I.; Tilley, T. D., Efficient C–H bond activations via O2 cleavage by a dianionic cobalt(ii) complex. *Chem. Sci.* **2014,** *5*, 2874-2878.
64. Goedken, V. L.; Kildahl, N. K.; Busch, D. H., Five-Coordinate Cobalt(II) Complexes of Macrocyclic Ligands — A New Reversible Oxygen Carrying System. *J. Coord. Chem.* **1977,** *7*, 89-103.
65. Jones, R. D.; Summerville, D. A.; Basolo, F., Synthetic oxygen carriers related to biological systems. *Chem. Rev.* **1979,** *79*, 139-179.
66. Busch, D. H.; Alcock, N. W., Iron and Cobalt "Lacunar" Complexes as Dioxygen Carriers. *Chem. Rev.* **1994,** *94*, 585-623.
67. Martin, D. J.; Wise, C. F.; Pegis, M. L.; Mayer, J. M., Developing Scaling Relationships for Molecular Electrocatalysis through Studies of Fe-Porphyrin-Catalyzed O2 Reduction. *Acc. Chem. Res.* **2020,** *53*, 1056-1065.
68. Matsubara, Y., Unified Benchmarking of Electrocatalysts in Noninnocent Second Coordination

Spheres for CO2 Reduction. *ACS Energy Lett.* **2019,** *4*, 1999-2004.

TOC Figure:

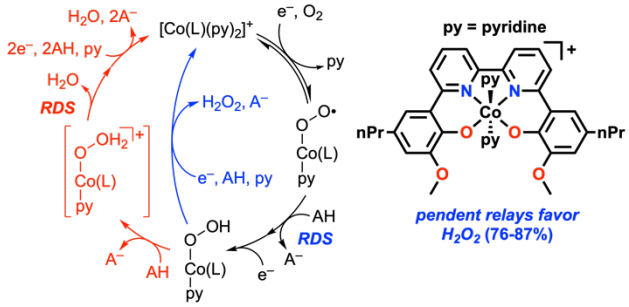
H2O, 2A−
2e−, 2AH, py
H2O
RDS
[Co(L)(py)2]+
e−, O2
py
H2O2, A−
e−, AH, py
AH
RDS
A−
e−
A−
AH
py = pyridine
pendent relays favor
H2O2 (76-87%)